UNIVERSITY OF BIRMINGHAM
University of Birmingham Research at Birmingham

Ambient air particulate total lung deposited surface area (LDSA) levels in urban Europe

Liu, Xiansheng; Hadiatullah, Hadiatullah; Zhang, Xun; Trechera, Pedro; Savadkoohi, Marjan; Garcia-Marlès, Meritxell; Reche, Cristina; Pérez, Noemí; Beddows, David C.S.; Salma, Imre; Thén, Wanda; Kalkavouras, Panayiotis; Mihalopoulos, Nikos; Hueglin, Christoph; Green, David C.; Tremper, Anja H.; Chazeau, Benjamin; Gille, Grégory; Marchand, Nicolas; Niemi, Jarkko V.

Link to publication on Research at Birmingham portal

Ambient air particulate total lung deposited surface area (LDSA) levels in urban Europe

Xiansheng Liu [a,*], Hadiatullah Hadiatullah [b], Xun Zhang [c,d,*], Pedro Trechera [a], Marjan Savadkoohi [a,e], Meritxell Garcia-Marlès [a,f], Cristina Reche [a], Noemí Pérez [a], David C.S. Beddows [h], Imre Salma [h], Wanda Thén [i], Panayiotis Kalkavouras [j,k], Nikos Mihalopoulos [j,k], Christoph Hueglin [l], David C. Green [m,n], Anja H. Tremper [m], Benjamin Chazeau [o,p], Grégory Gille [q], Nicolas Marchand [o], Jarkko V. Niemi [r], Hanna E. Manninen [r], Harri Portin [r], Nadezda Zikova [s], Jakub Ondracek [s], Michael Norman [t], Holger Gerwig [u], Susanne Bastian [v], Maik Merkel [w], Kay Weinhold [w], Andrea Casans [x], Juan Andrés Casquero-Vera [a,x], Francisco J. Gómez-Moreno [y], Begoña Artíñano [y], Maria Gini [z], Evangelia Diapouli [z], Suzanne Crumeyrolle [aa], Véronique Riffault [ab], Jean-Eudes Petit [ac], Olivier Favez [ad], Jean-Philippe Putaud [ae], Sebastiao Martins Dos Santos [ae], Hilkka Timonen [af], Pasi P. Aalto [ag], Tareq Hussein [ag,ah], Janne Lampilahti [ag], Philip K. Hopke [ai], Alfred Wiedensohler [w], Roy M. Harrison [g,aj], Tuukka Petäjä [ag], Marco Pandolfi [a], Andrés Alastuey [a], Xavier Querol [a]

[a] Institute of Environmental Assessment and Water Research (IDAEA-CSIC), Barcelona, Spain
[b] School of Pharmaceutical Science and Technology, Tianjin University, Tianjin, China
[c] Beijing Key Laboratory of Big Data Technology for Food Safety, School of Computer Science and Engineering, Beijing Technology and Business University, Beijing, China
[d] Hotan Normal College. Hotan 848000, Xinjiang, China
[e] Department of Mining, Industrial and ICT Engineering (EMIT), Manresa School of Engineering (EPSEM), Universitat Politècnica de Catalunya (UPC), 08242 Manresa, Spain
[f] Department of Applied Physics-Meteorology, University of Barcelona, Barcelona, Spain
[g] Division of Environmental Health and Risk Management, School of Geography, Earth and Environmental Sciences University of Birmingham, Edgbaston, Birmingham, United Kingdom
[h] Institute of Chemistry, Eötvös Loránd University, Budapest, Hungary
[i] Hevesy György Ph.D. School of Chemistry, Eötvös Loránd University, Budapest, Hungary
[j] Environmental Chemical Processes Laboratory, Department of Chemistry, University of Crete, Heraklion, Greece
[k] Institute for Environmental Research & Sustainable Development, National Observatory of Athens, Athens, Greece
[l] Laboratory for Air Pollution and Environmental Technology, Swiss Federal Laboratories for Materials Science and Technology (EMPA), Duebendorf, Switzerland
[m] MRC Centre for Environment and Health, Environmental Research Group, Imperial College London, UK
[n] NIHR HPRU in Environmental Exposures and Health, Imperial College London, UK
[o] Aix Marseille Univ., CNRS, LCE, Marseille, France
[p] Laboratory of Atmospheric Chemistry, Paul Scherrer Institute, Villigen, Switzerland
[q] AtmoSud, Regional Network for Air Quality Monitoring of Provence-Alpes-Côte-d'Azur, Marseille, France
[r] Helsinki Region Environmental Services Authority (HSY), Helsinki, Finland
[s] Institute of Chemical Process Fundamentals, v.v.i. Academy of Sciences of the Czech Republic Rozvojova, Prague, Czech Republic
[t] Environment and Health Administration, SLB-analys, Stockholm, Sweden
[u] German Environment Agency (UBA), Dessau-Roßlau, Germany
[v] Saxon State Office for Environment, Agriculture and Geology (LfULG), Dresden, Germany
[w] Leibniz Institute for Tropospheric Research (TROPOS), Leipzig, Germany
[x] Andalusian Institute for Earth System Research (IISTA-CEAMA), University of Granada, Granada, Spain
[y] Department of Environment, CIEMAT, Madrid, Spain
[z] ENRACT, Institute of Nuclear and Radiological Science & Technology, Energy & Safety, NCSR Demokritos, 15310 Ag. Paraskevi, Athens, Greece
[aa] Univ. Lille, CNRS, UMR 8518 Laboratoire d'Optique Atmosphérique (LOA), Lille, France
[ab] IMT Nord Europe, Institut Mines-Télécom, Université de Lille, Centre for Energy and Environment, 59000, Lille, France
[ac] Laboratoire des Sciences du Climat et de l'Environnement, CEA/Orme des Merisiers, Gif-sur-Yvette, France
[ad] Institut national de l'environnement industriel et des risques (INERIS), Parc Technologique Alata BP2, Verneuil-en-Halatte, France
[ae] European Commission, Joint Research Centre (JRC), Ispra, Italy
[af] Atmospheric Composition Research, Finnish Meteorological Institute, Helsinki, Finland
[ag] Institute for Atmospheric and Earth System Research (INAR), Faculty of Science, University of Helsinki, Finland
[ah] Environmental and Atmospheric Research Laboratory, Department of Physics, School of Science, The University of Jordan, Amman 11942, Jordan
[ai] Department of Public Health Sciences, University of Rochester School of Medicine and Dentistry, Rochester, NY, USA
[aj] Department of Environmental Sciences, Faculty of Meteorology, Environment and Arid Land Agriculture, King Abdulaziz University, Jeddah, Saudi Arabia

* Corresponding authors.
  E-mail addresses: liugar@cid.csic.es (X. Liu), zhangxun@btbu.edu.cn (X. Zhang).

HIGHLIGHTS

- Lung deposited surface area (LDSA) was investigated in 25 EU and one USA sites.
- Peaks of total LDSA were recorded in 06:00–8:00 and 19:00–22:00 UTC in urban.
- The seasonal changes of LDSA showed significant differences in its levels ($p < 0.01$).
- Aitken and Accumulation mode particles play a significant role in the total LDSA.

GRAPHICAL ABSTRACT
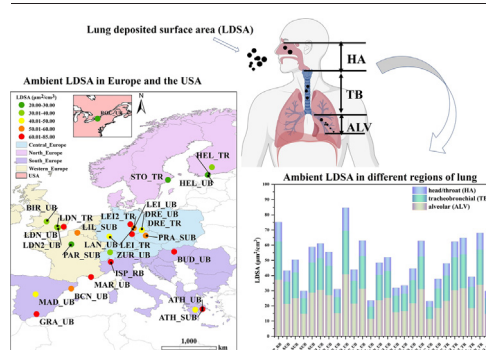
ARTICLE INFO

ABSTRACT

This study aims to picture the phenomenology of urban ambient total lung deposited surface area (LDSA) (including head/throat (HA), tracheobronchial (TB), and alveolar (ALV) regions) based on multiple path particle dosimetry (MPPD) model during 2017–2019 period collected from urban background (UB, $n = 15$), traffic (TR, $n = 6$), suburban background (SUB, $n = 4$), and regional background (RB, n = 1) monitoring sites in Europe (25) and USA (1). Briefly, the spatial-temporal distribution characteristics of the deposition of LDSA, including diel, weekly, and seasonal patterns, were analyzed. Then, the relationship between LDSA and other air quality metrics at each monitoring site was investigated. The result showed that the peak concentrations of LDSA at UB and TR sites are commonly observed in the morning (06:00–8:00 UTC) and late evening (19:00–22:00 UTC), coinciding with traffic rush hours, biomass burning, and atmospheric stagnation periods. The only LDSA night-time peaks are observed on weekends. Due to the variability of emission sources and meteorology, the seasonal variability of the LDSA concentration revealed significant differences ($p = 0.01$) between the four seasons at all monitoring sites. Meanwhile, the correlations of LDSA with other pollutant metrics suggested that Aitken and accumulation mode particles play a significant role in the total LDSA concentration. The results also indicated that the main proportion of total LDSA is attributed to the ALV fraction (50 %), followed by the TB (34 %) and HA (16 %). Overall, this study provides valuable information of LDSA as a predictor in epidemiological studies and for the first time presenting total LDSA in a variety of European urban environments.

1. Introduction

With the rapid development of the economy, energy consumption has been on the rise, generating a large volume of emissions into the atmosphere, causing serious air pollution issues (Khan et al., 2022). The atmospheric aerosol (particulate matter, PM), constitutes an important fraction of air pollution with major effects on public health (Mahowald et al., 2014; Rao et al., 2018; Wehner et al., 2002). The complex chemical composition of the aerosol particles, and their highly variable particle number size distributions (PNSD) confer physicochemical properties that might have various effects on human health (Baldauf et al., 2016; McMurry, 2000).

Epidemiological and toxicological studies have suggested that the smaller the particles, the more toxic they might be, especially ultrafine particulate matter (UFP, or particles smaller than 100 nm) (Kwon et al., 2020). Because of their small size, these might access deeper parts of the lungs, and even the bloodstream through lung translocation, thus causing systemic toxicity (Cassee et al., 2019; Salma et al., 2015; Vieira and Koutrakis, 2021). These UFPs also have a larger surface area for the same mass than accumulation and coarse mode particles have. As a result, they can potentially carry more harmful substances into the alveoli and circulatory system, having a greater toxic effect than large diameter particles (Abdillah and Wang, 2022; Chen et al., 2016; Sioutas et al., 2005; Sun et al., 2019). Nowadays, a widely used approach to combine the lung deposition and surface area of particles is to measure or calculate the concentrations of lung deposited surface area (LDSA).

The determination of LDSA is of high interest for exposure assessment, as it reflects the concept that particle surface area available in the lung is a relevant exposure metric. LDSA has been proposed as a critical predictor for health outcomes from aerosol exposure, as it appears to be one of the most relevant physical metrics for evaluating exposure to particles (Chang et al., 2022; Schmid and Stoeger, 2016). In prior studies, LDSA concentrations have been reported for ambient aerosols in different environments and several cities in the world. For instance, ambient measurements have been conducted in Barcelona (Spain) (Reche et al., 2015), Helsinki (Finland) (Fung et al., 2022; Kuuluvainen et al., 2016), Leicester (Hama et al., 2017), Beijing (China) (Xu et al., 2022), Augsburg (Germany) (Liu et al., 2022), and Minneapolis (USA) (Gonzalez et al., 2022). However, comparative data for total LDSA concentrations deposited in the all regions of lung for different site typologies (urban background, UB; traffic, TR; suburban background, SUB; and regional background, RB, areas) are still very limited and needed.

Herein, we explored total LDSA concentrations within European cities in the framework of the RI-URBANS project (Research Infrastructures Services Reinforcing Air Quality Monitoring Capacities in European Urban & Industrial Areas). We conducted an analysis using hourly PNSDs measured from 25 monitoring sites in Europe and one in the USA between 2017 and 2019 (the compiled datasets of particle number size distributions, SI, Table S1) to estimate the regional deposition of LDSA in the head/throat (HA), tracheobronchial (TB), and alveolar (ALV) regions of the human respiratory system. We also investigated the spatial-temporal distribution characteristics of the deposition, including diel, weekly, and seasonal patterns. In addition, the spatial and seasonal heterogeneity levels of the monitoring stations were analyzed using a coefficient of divergence (COD). Finally, the relationship between LDSA and other air quality metrics,

namely particle number concentration (PNC) in different modes (nucleation, Aitken, accumulation), black carbon (BC), gaseous pollutants (SO_2, NO, NO_2, O_3, and CO) and PM_1, $PM_{2.5}$, PM_{10} at each monitoring site was investigated to reveal the essential metrics associated with LDSA, identifying the most closely metrics are associated with LDSA, and thus providing insights into the sources and transport of LDSA and its potential impacts on human health and the environment. Overall, this study provides valuable information for use in an evaluation of the health effects of atmospheric aerosol particles, including UFP.

2. Methods

2.1. Instrumentation

The instrumentation used for measuring all metrics at the different stations is described in Table S1. Different instruments and measuring configurations were used for PNSD measurements at the different sites. Briefly, in this study the PNSDs were measured by Mobility Particle Size Spectrometers (MPSS) (Table S1). BC concentrations were monitored either by a Multi-Angle Absorption Photometer (MAAP, Thermo Scientific model 5012) or a multi-wavelength Aethalometer (Magee Scientific, Model AE33/21, Slovenia) (Table S1). To ensure data quality, we conducted a number of data QA/QC procedures. We applied a data completeness filter to exclude data with poor availability. Furthermore, we performed a sensor agreement check to ensure consistency between the MPSS and other particle instruments such as the Scanning Mobility Particle Sizers (SMPS).

Concentrations of PM_X (PM_1, $PM_{2.5}$, PM_{10}) and of the above referred gaseous pollutants were measured with the conventional instrumentation used in Europe and the US for air quality monitoring. Specifically, PM_X were measured using a Tapered Element Oscillating Microbalance (TEOM, R&P 1400a, Thermo Scientific™), while gaseous pollutants including NO/NO_2, O_3, SO_2, and CO are generally recorded by commercial instruments with the use of the chemiluminescence, UV-absorption, UV-fluorescence, and gas filter correlation techniques, respectively.

2.2. Calculation of the size-fractionated lung-deposited surface area (LDSA)

The method commonly used to determine the geometric surface area concentration of spherical particles is based on the measurement of PNSD (Asbach et al., 2009; Fierz et al., 2011). Particles produced from combustion typically form chain-like structures (McDonald and Biswas, 2004), which can have a higher porosity and surface area than spherical particles. Therefore, the assumption of spherical particle shape used in this study is an approximation and may underestimate the total surface area. In the case of spherical particles, the PNSD can be easily converted into surface area size distributions (SASD) by means of the known relationship between a sphere's surface area and its diameter. These distributions can be integrated over the size range of interest to obtain the total surface area concentrations. Following that, to obtain LDSA concentrations, the SASDs can be weighted with lung deposition curves (Hussein et al., 2013) and integrated over the size range of interest. In this study, a model was applied to divide the respiratory tract into three main regions, including HA, TB, and ALV regions, based on the multiple path particle dosimetry (MPPD) models (Asgharian, 2022; Hussein et al., 2013; Hussein et al., 2015). In our calculations, we used size-dependent regional deposition fraction (DF) curves obtained from MPPD software (version 3.04, Chemical Industry Institute of Toxicology, Research Triangle Park, NC; https://www.ara.com/mppd/). The total LDSA values were calculated by first counting the number of particles in each size bin and then multiplying the PNC with the specific deposition fraction of the given particle size. To accurately assess the contributions of LDSA, it is important to consider the particle sizes involved. As depicted in Fig. S1, particles smaller than 10 nm have a relatively low weight in the overall calculation of LDSA contributions (0.14 % ± 0.2 %), compared to other particle sizes. In our study we also compared the values of ALV-LDSA by MPPD and lung-deposited Nanoparticle Surface Area Monitor (NSAM) (TSI, Model 3550, USA). The comparison showed a

very good agreement of the results (Pearson's r^2 = 0.927, Fig. S2), further indicating that the MPPD can be used to estimate the LDSA concentration.

2.3. Statistical analysis

The metrics are reported as average concentration (AVE) ± standard deviation (STD). The correlations between LDSA and other metrics for the different periods were analyzed by calculation of Pearson's correlation coefficient. The statistically significant differences in LDSA concentrations in a different time (diel, weekly, and seasonal) and 26 monitoring sites were studied using the Kruskal-Wallis ANOVA on ranks (Kruskal and Wallis, 1952) and Duncan's Multiple Range Test (Duncan, 1955), which was performed using SPSS Software (IBM SPSS Statistics 25, Chicago, IL, USA). Subsequently, due to data on air pollutants also exhibit the same characteristics as geospatial data (i.e., spatial heterogeneity) (Yang et al., 2018), a coefficient of divergence (COD) was applied to analyse the spatial and seasonal heterogeneity of ambient pollutants (Faridi et al., 2019). The COD_{jk} method for identifying the differences was described in the SI (-Section 1.3). Spatially, it has been suggested that a low COD_{jk} value (<0.2) indicates a high level of homogeneity between sites, while a high COD_{jk} value (>0.2) indicates heterogeneous sites (Wilson et al., 2005).

3. Result and discussion

3.1. General characteristics of total LDSA at different measurement sites

The hourly total concentration of LDSA was examined for the years 2017–2019 using Kruskal-Wallis ANOVA analysis and Duncan's method. The results revealed that some sites (e.g., BCN_UB, LEI_UB, and ATH_UB, among others) were significantly different from the other ones, while some sites' pairs (e.g., ROC_UB and HEL_UB) suggested similar behaviour (Table S2 and S3). These differences indicate that there are both spatial heterogeneity and homogeneity across the various monitoring locations. Furthermore, our results show that the average COD_{jk} is 0.32 ± 0.06 at UB stations, indicating the high spatial heterogeneity between these monitoring sites (COD_{jk} > 0.2). The lower COD_{jk} values are found in the SUB/RB (average COD_{jk}, 0.28 ± 0.06) and TR (average COD_{jk}, 0.26 ± 0.05) (SI, section 2.1, Fig. S3), suggesting a certain extent of homogeneity between these monitoring site. As a result, these findings may be useful in identifying the potential sources of LDSA and developing common but also site-specific strategies to mitigate its impacts on human health and the environment.

In addition, comparing all monitoring sites (Table S4), for UB areas, the highest annual average total LDSA concentration is found in BUD_UB (85 ± 53 $\mu m^2/cm^3$), followed by GRA_UB and MAR_UB (63 ± 47, 63 ± 48 $\mu m^2/cm^3$), while the lowest is in ROC_UB (23 ± 15 $\mu m^2/cm^3$) and HEL_UB (24 ± 16 $\mu m^2/cm^3$). For TR site, the highest annual average total LDSA is found in LDN_TR (68 ± 41 $\mu m^2/cm^3$), followed by LEI2_TR (65 ± 39 $\mu m^2/cm^3$), while the lowest is in STO_TR (30 ± 16 $\mu m^2/cm^3$) and HEL_TR (39 ± 26 $\mu m^2/cm^3$). For SUB areas, the highest annual average total LDSA is found in PRA_SUB (59 ± 81 $\mu m^2/cm^3$), followed by LIL_SUB (50 ± 34 $\mu m^2/cm^3$), while the lowest is in ATH_SUB (43 ± 24 $\mu m^2/cm^3$) and PAR_SUB (30 ± 22 $\mu m^2/cm^3$). The high STD associated with the annual average total LDSA concentrations could be mainly attributed to diel variations in emissions sources, meteorological conditions, and transport patterns. The differences could partly also be influenced by the correction method applied for particle diffusion losses in the MPSSs. In Budapest, a conservative size-independent method is applied which resulted in a correction factor of 1.22–1.27 over the 3 years (Salma et al., 2016). Interestingly, ISP_RB, located in an air pollution hotspot region of Europe (the Po Valley) also had the second highest total LDSA concentration (75 ± 61 $\mu m^2/cm^3$) of all monitoring sites. Overall, the highest concentration of total LDSA is found in UB (BUD_UB) and the lowest is also found in UB (HEL_UB), which is comparable with the trend of $PM_{2.5}$ (Fig. 1, Fig. S4, and Table S2).

Moreover, the contributions to the deposition of annual average total LDSA in different regions of the respiratory tract, including HA, TB, and
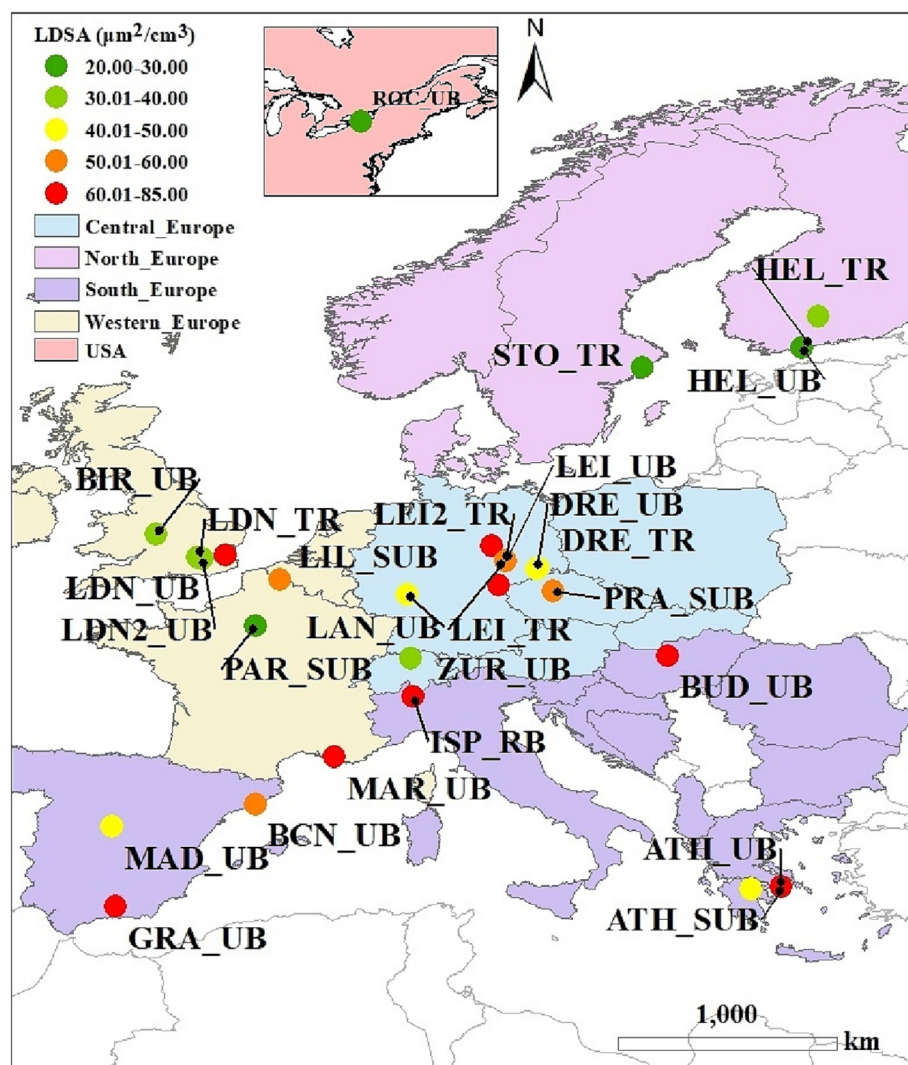
Fig. 1. 2017–2019 average concentrations of total LDSA at 25 European sites and one from the USA.

ALV, are also estimated at all research sites during the observed period (Table S2). The results of the total LDSA concentration calculations show that LDSA is primarily accumulated in ALV (50 %), which is considered to present the greatest potential health risk (Fung et al., 2022; Salo et al., 2021a,Salo et al., 2021b), and lower contributions were obtained for HA (16 %) and TB (34 %) deposition, consistent with the strong size-dependence of deposition (Kumar et al., 2014; Voliotis and Samara, 2018). A previous study reporting an estimation for the inhaled deposited dose rate during common exposure scenarios for UB aerosols in an Eastern Mediterranean city (Amman, Jordan), reported HA, TB, and ALV inhaled deposited doses reaching 7–16 %, 16–28 %, and 56–76 %, respectively (Hussein et al., 2022). In comparison, a prior study in the Helsinki metropolitan area found that the annual mean ALV-LDSA concentrations varied between 9 and 22 μm^2/cm^3 at different sites (Kuula et al., 2020). The range was 9–12 μm^2/cm^3 for urban background and detached housing area sites, which are quite clean areas in Helsinki (Kuula et al., 2020), to values up to ~189 μm^2/cm^3 typically observed near PM sources such as urban roads in Athens, Greece (Cheristanidis et al., 2020). This range was confirmed by our results where the ALV-LDSA annual averages range from 12 ± 8 to 41 ± 29 μm^2/cm^3, pointing to a significant heterogeneity of LDSA across urban Europe. In addition, a recent study on the different locations of BC in the lungs, also showed BC was majorly deposited in the ALV region, accounting for 49.0–53.2 % of the total BC deposition dose, less in the TB region (35.6–37.2 %) and even less in the HA region, 11.2–13.8 % (Liu et al., 2023).

3.2. Total LDSA time trends

3.2.1. Diel variations

Diel variation in total LDSA can be used as an indicator of the role of local human activities, effects of meteorology and exposure to air pollution risks (Reddy et al., 2012; Zhou et al., 2018). The results showed that the diel trends of total LDSA revealed some similar features among all monitoring sites (Fig. 2 and Fig. S5). At the UB sites (Fig. 2a and Fig. S5a), the morning peak of total LDSA occurred at ~06:00–09:00 UTC, approximately one hour after local sunrise. The former coincided with the morning traffic rush hours (Teinilä et al., 2019). For example, the total LDSA concentrations in BUD_UB are significantly ($p = 0.0001$) higher than in the other cities, which may be closely related to the residential and household emissions, industrial sources, and some off-road transport, types of vehicles, traffic flow, and long-range transport of air masses in that city (Salma et al., 2017; Salma et al., 2020; Thén and Salma, 2022). A prior study also reported that during rush hour, about 74 % of LDSA is attributed to traffic emitted particles (Chang et al., 2022). Furthermore, it is also worth noting that the morning peak of LDSA at TR sites starts earlier (4:30–6:00 UTC), is more pronounced, remains high until the evening traffic peak (~19:00 UTC), and then slightly decreases (Fig. 2c & S5c), further illustrating the impact of traffic on total LDSA (Reche et al., 2015; Wierzbicka et al., 2014). Then, after the morning peak, at UB sites, the total LDSA is reduced due to a decrease in emissions and relative humidity (RH), and increased temperature (T), wind speed (WS), and radiation (RAD) (Fig. S6). The
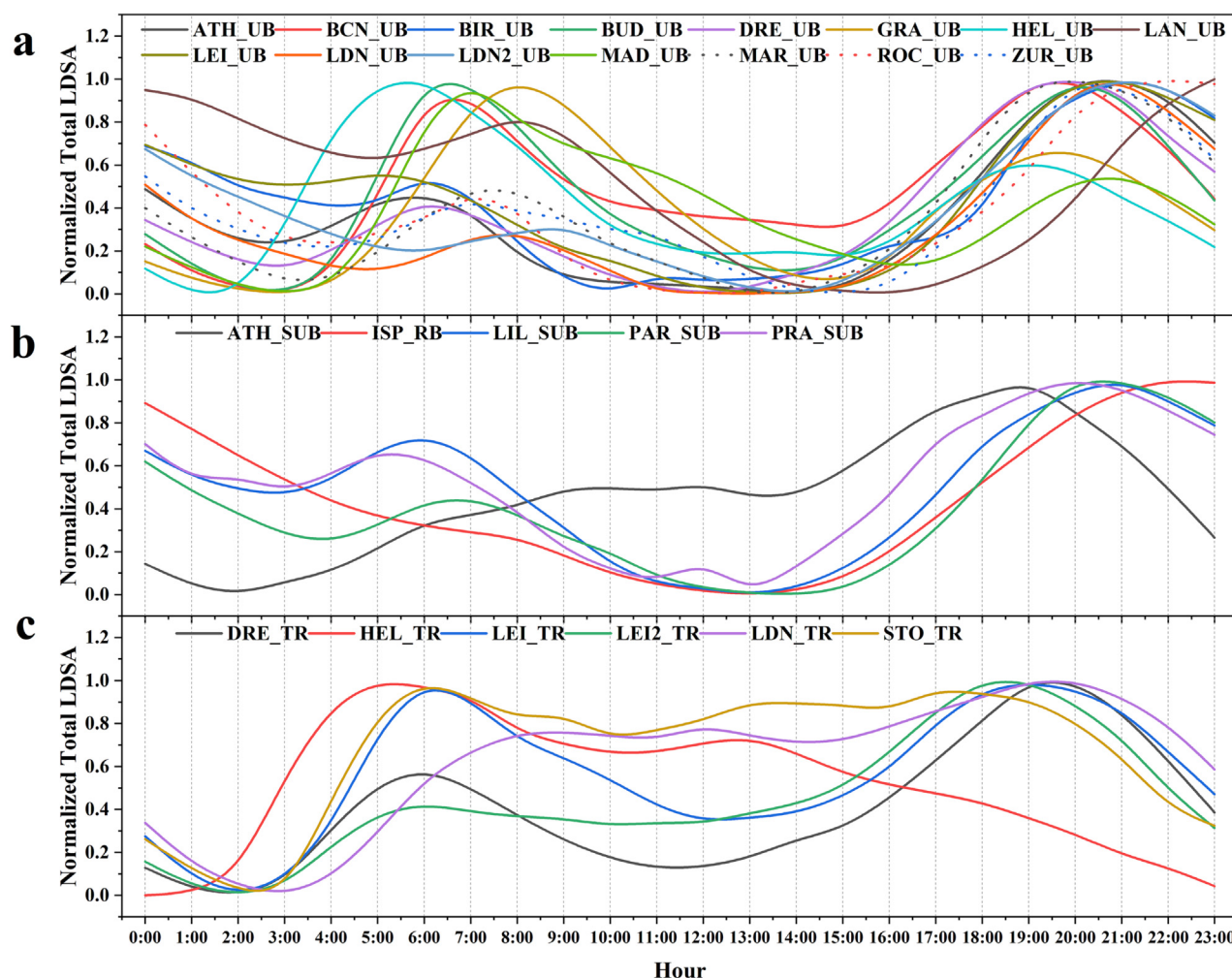
Fig. 2. 2017–2019 average of normalized hourly total LDSA for the 26 studied sites. a, urban background (UB) sites; b, suburban background (SUB) and regional background (ISP_RB) sites; and c, traffic (TR) sites (Min-Max normalization was used in a dataset to fall within a specified range, typically between 0 and 1. It is calculated by subtracting the minimum value in the dataset from each value and dividing by the range of the dataset).

lowest concentrations are usually detected in the midday-afternoon (12:00–16:00 UTC) at all background sites due to less from traffic (or biomass burning in winter) for these hours, higher WS and increased mixing depth (Fig. S6d, g), thus increasing dispersion conditions.

After 16:00 UTC, which majorly leave from work, traffic increases and a broad LDSA evening peak regularly is observed between ~19:00–22:00 UTC at UB and TR sites (Fig. 2). However, at HEL_TR, it is hardly affected by the rush hour at evening. This difference is mainly due to the fact that the site is less affected by residential heating and the homecoming traffic at evening (Helin et al., 2018; Hietikko et al., 2018). It was also found in the previous study of diel variation in black carbon at this site (Helin et al., 2018). The latter total LDSA peaks during these hours might be linked to increased vehicular emissions associated with evening traffic rush hour (Chang et al., 2022), cooking (Allan et al., 2010), and biomass burning (particularly during winter) (Bari et al., 2010; Liu et al., 2022), as well as unfavorable meteorological conditions (e.g., low WS and greater stability and reduced mixing depth, Fig. S6) for dispersion (Zhu et al., 2018). The slight decreasing trend from midnight to early morning (23:00 to 03:00 UTC, Fig. 2) is attributed to the progressive reduction of anthropogenic emissions, including traffic flow. Meanwhile, during this period, there is the potential for hygroscopic particles to absorb water when the RH increases, which can increase the particle size, leading to a decrease in total LDSA (Li et al., 2021; Wiegand et al., 2011).

For the SUB and RB sites, the diel variation of total LDSA is slightly different compared to UB and TR sites. A low peak of total LDSA is found in the

morning and evening traffic rush hours (05:00–06:00 and 19:00–20:00 UTC). Around those SUB sites, there are smaller roads with lighter traffic. Thus, at these locations, measurements are not significantly affected by direct and local fresh traffic emissions and trends are like the ones reported previously for this environment (Kuuluvainen et al., 2016). Thus, LDSA tends to be quite constant with very narrow variations (± 5 μm²/cm³) along the day (Fig. 2b). In contrast, at ISP_RB, the total LDSA concentration gradually decreases from 0:00–15:00 UTC and increases during the evening (21:00–0:00 UTC), with a ± 16 μm²/cm³ average hourly variation, which may be caused by marked nocturnal thermal inversions in the Po Valley, characterized by extremely low winds, due to the Alps' protection against northern winds, and high wintertime biomass burning domestic emissions.

3.2.2. Weekly variations

The weekly average variations of the total LDSA concentrations at UB and TR sites (Fig. 3) are characterized by higher workday (Monday-Friday) values, when the highest total LDSA concentration is measured during morning and evening rush hours (6:00–9:00 and 18:00–21:00 UTC) due to the high vehicle-exhaust emissions (Reche et al., 2015). In the weekend (Saturday and Sunday), for urban areas, there is a significant decrease (Fig. 3a, c). During weekend mornings, there are no or weak total LDSA peaks (Fig. 3a, c) because of the low traffic density, excluding GRA_UB sites. However, only a later peak is found on Saturday and Sunday evenings (~20:00–22:00 UTC) compared to the corresponding peak on weekdays, due to high recreational mobility and higher emissions from cooking and
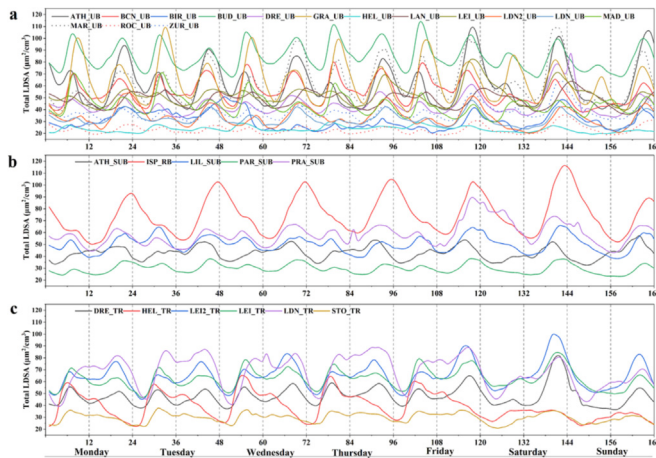
Fig. 3. 2017–2019 hourly total LDSA averaged concentrations per day of the week for the 26 studied sites. a, urban background (UB) sites; b, suburban background (SUB) and regional background (ISP_RB) sites; and c, traffic (TR) sites.

domestic heating when people stay at home during weekends (Allan et al., 2010). Additional weekend contributions to total LDSA stem from events such as barbecues and late-night activities on Saturdays, resulting in a peak occurring later in the day and lasting for longer (Hama et al., 2017).

At the SUB/RB sites (Fig. 3b), the weekly diel trend for total LDSA has a weak morning peak and a more pronounced evening peak, which is comparable with urban sites (see the highest averaged total LDSA concentrations on Saturday midnight at ISP_RB, Fig. 3b, probably due to recreational domestic biomass burning or longer use of heating).

3.2.3. Seasonal variations

Fig. 4 shows the 2017–2019 average hourly total LDSA concentrations by season (Spring, Mar-May; Summer, Jun-Aug; Autumn, Sep-Nov; Winter, Dec-Feb) for each site. Overall, the total LDSA concentrations at all monitoring sites showed substantial seasonal differences ($p = 0.05$, Table S5). The extent to which there were statistically significant differences in total LDSA concentrations between seasons varied slightly across different monitoring sites. For example, BUD_UB, ISP_RB, LAN_UB, and MAD_UB were significantly different between the four seasons ($p = 0.0001$), while the total LDSA concentrations at ATU_SUB, HEL_UB, HEL_TR, LER2_TR, and ROC_UB were not different between the autumn and winter seasons, and ATH_SUB, GRA_UB, LDSA concentrations at the ATH_SUB, GRA_UB, LER2_TR, and PAR_SUB, sites did not differ significantly between the spring and summer seasons, further suggesting that LDSA is influenced by local pollution sources. In addition, combined with the COD analysis for seasonal variability, the seasonal heterogeneous among all sites were mainly found between winter and other three seasons, specially between winter and summer (0.29 ± 0.12 for SUB, 0.30 ± 0.06 for UB, and 0.12 ± 0.04 for TR) (SI, section 2.2, Fig. S7), indicating that meteorological conditions (e.g., temperature) has a strong influence on air pollution at UB and SUB ($COD_{jk} > 0.2$). However, it is worth noting that at TR sites, the seasonal variation of air pollution shows homogeneity ($COD_{jk} < 0.2$), which indicates that TR sites are a relatively stable source of pollution, and the frequency and routes of vehicle operations do not change much, so the stability of the pollution source may lead to little difference in seasonal variation.

In winter, the highest average exposures to LDSA metrics are found at ATH_UB, BUD_UB, GRA_UB, LDN2_UB, MAD_UB, ZUR_UB, DRE_TR, ISP_RB, PAR_SUB, and PRA_SUB. The increase in total LDSA concentration in winter may be influenced by the emissions from residential heating, traffic emissions, and meteorological conditions favoring stagnation (Liu et al., 2021a,Liu et al., 2021b). For example, (Katsanos et al., 2019) reported a significant enhancement of biomass burning aerosols at the ATH_UB site in winter (12/2016–02/2017) and revealed that organic matter contributed approximately half of the submicron mass in winter, which also influenced with lower WS (<3 m/s), enhancing the winter aerosol load. The

analysis of seasonal meteorological factors indicates that lower winter temperatures in cities such as BUD_UB, ISP_RB, and MAD_UB, which are predominantly affected by temperature, can result in elevated surface air pollution. This is mainly due to increased heating of homes during colder seasons combined with lasting T inversion layers occurring in the whole Carpathian Basin in winter. The latter phenomenon restricts the vertical and horizontal air mixing and results in poor air quality over extended areas of the basin in larger and smaller cities as well as in rural areas. Additionally, an earlier study conducted in Budapest revealed that biomass burning is the primary source of air pollution in winter, accounting for ca. 70 % of the total carbon emissions in the $PM_{2.5}$ size fraction (Salma et al., 2020). While in Madrid's winter evenings, temperature inversion traps polluted air under a warm air layer, causing smog and poor air quality (Siegmann and Gomez-Moreno, 2022).

The highest average exposure to total LDSA metrics at different sites vary seasonally, possibly due to differences in PNSD. During summer, sites such as BCN_UB, HEL_UB, LAN_UB, LDN_UB, ROC_UB, LIL_SUB, HEL_TR, and STO_TR have the highest average total LDSA, while during spring, DRE_UB, LEI_UB, LEI_TR, LEI2_TR, and LDN_TR have the highest average total LDSA. Previous research by (Masiol et al., 2018) found Accumulation mode PNC peaked at the ROC_UB site in summer due to increased photochemical activity leading to more secondary particle formation, this phenomenon was also observed in Germany (e.g., Dresden, Berlin, etc.) (Junkermann et al., 2016). In addition, in Helsinki, Finland (e.g., HEL_UB, HEL_TR), it may be due to long-range atmospheric transport and vertical downward transport from high altitude atmospheric layers enriched in nucleation and Aitken mode particles (Lampilahti et al., 2021; Niemi et al., 2009; Petzold et al., 2008). Finally, in Barcelona (BCN_UB), factors such as burning and forest fires, shipping, and aviation may contribute to high total LDSA in summer (Petzold et al., 2008; Rivas et al., 2020). Due to the lack of complete annual data for BIR_UB and MAR_UB, no comparison of seasonal exposure has been made.

3.3. Total LDSA vs other metrics

3.3.1. Total LDSA vs fine modes

In ambient air, particles are usually distributed across several overlapping "modes", i.e., the nucleation (1–25 nm), Aitken (25–100 nm), accumulation (100–1000 nm) and coarse (1000–10,000 nm) modes, rather than evenly distributed (Harrison et al., 2000; Whitby et al., 1972)(Harrison et al., 2000; Whitby et al., 1972). Particles from these modes have different formation mechanisms (or sources) as well as differing aerodynamic behavior and fate. Therefore, this study analyzes the correlations between total LDSA and fine modes, more specifically with nucleation (overall 10–25 nm, but varying from 10 to 25 nm to 20–25 nm, depending of the site, Table S1), Aitken (25–100 nm), and accumulation (100–500 nm) mode PNCs, and total PNC (10–500 nm).

As shown in Fig. 5, all the above modes had highly significant correlations with total LDSA ($p = 0.01$) in all sites. However, the correlations are higher for the accumulation mode ($r = 0.93 \pm 0.04$, max 0.98, min 0.84), followed by the Aitken mode ($r = 0.85 \pm 0.05$, max 0.94, min 0.77), N_{10-500} (PNC_{tot}) ($r = 0.84 \pm 0.09$, max 0.95, min 0.58), and lower for the nucleation mode ($r = 0.42 \pm 0.17$, max 0.89, min 0.13), suggesting that fine modes in the Aitken and accumulation have the greatest effect on the lung deposition. According to Seinfeld and Pandis (Seinfeld and Pandis, 2008) the most common size ranges for particle surface area is in the range of 100–500 nm, which was comparable with our study (Fig. S1). To measure the LDSA, one needs to measure the size distribution of particles and then calculate the particle surface in each size bin based on its lung-deposition probability. (Todea et al., 2015) conducted thorough measurements for several LDSA sensors and instruments (DiSCmini, Testo Inc.; nanoTracer, Philips Aerasense Inc.; Partector, Naneos Ltd.; NSAM 3550, TSI Inc.; Aerotrak, TSI Inc.). Additionally, previous studies by (Asbach et al., 2009) and (Hammer et al., 2019) have shown that particles smaller than the minimum of the deposition curves are more relevant to health effect studies, and LDSA concentrations are mainly influenced by
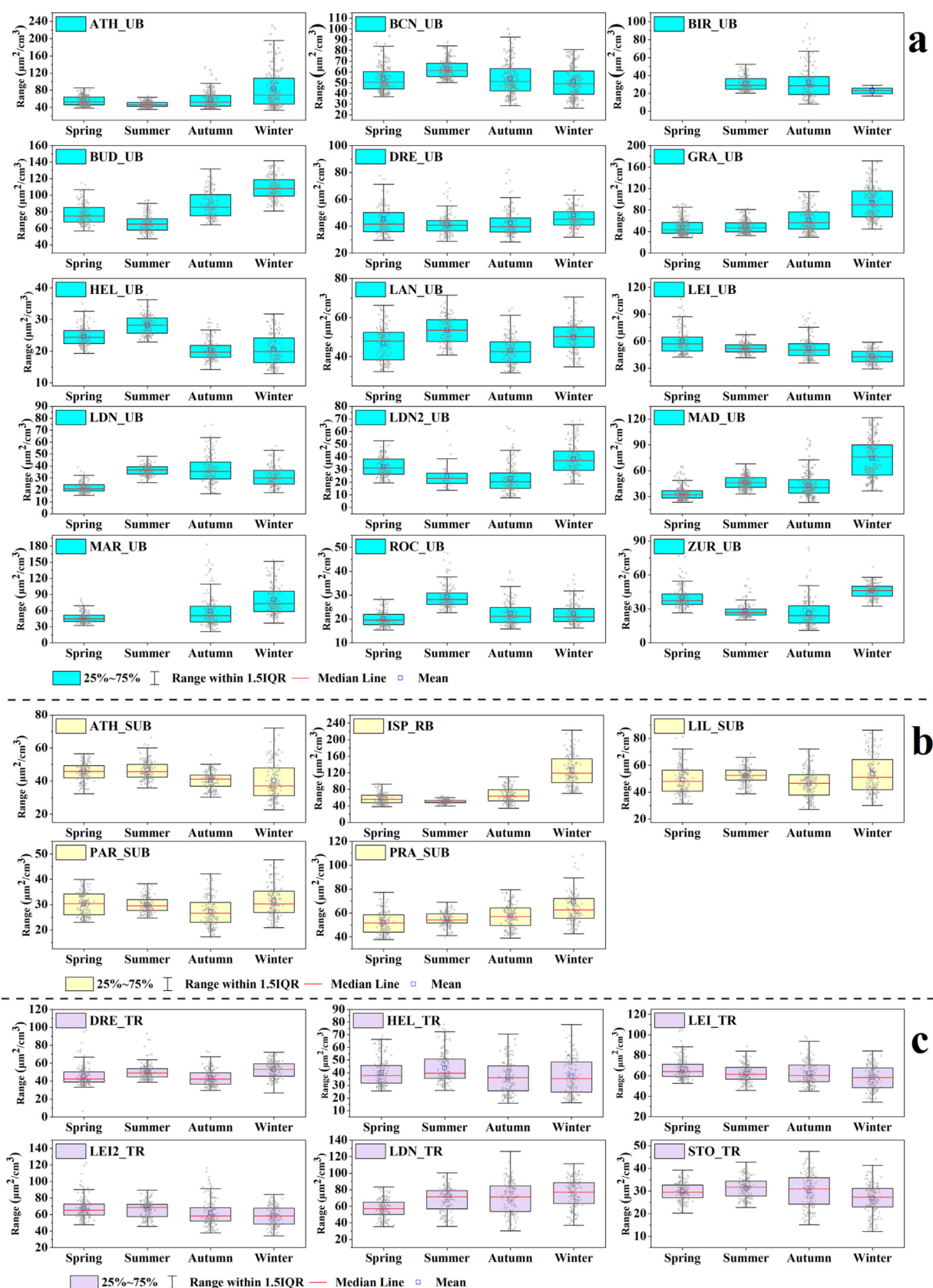
Fig. 4. 2017–2019 seasonal variations of total LDSA concentrations for 24 out of the 26 studied sites. a, urban background (UB) sites; b, suburban background (SUB) and regional background (ISP_RB) sites; and c, traffic (TR) sites.
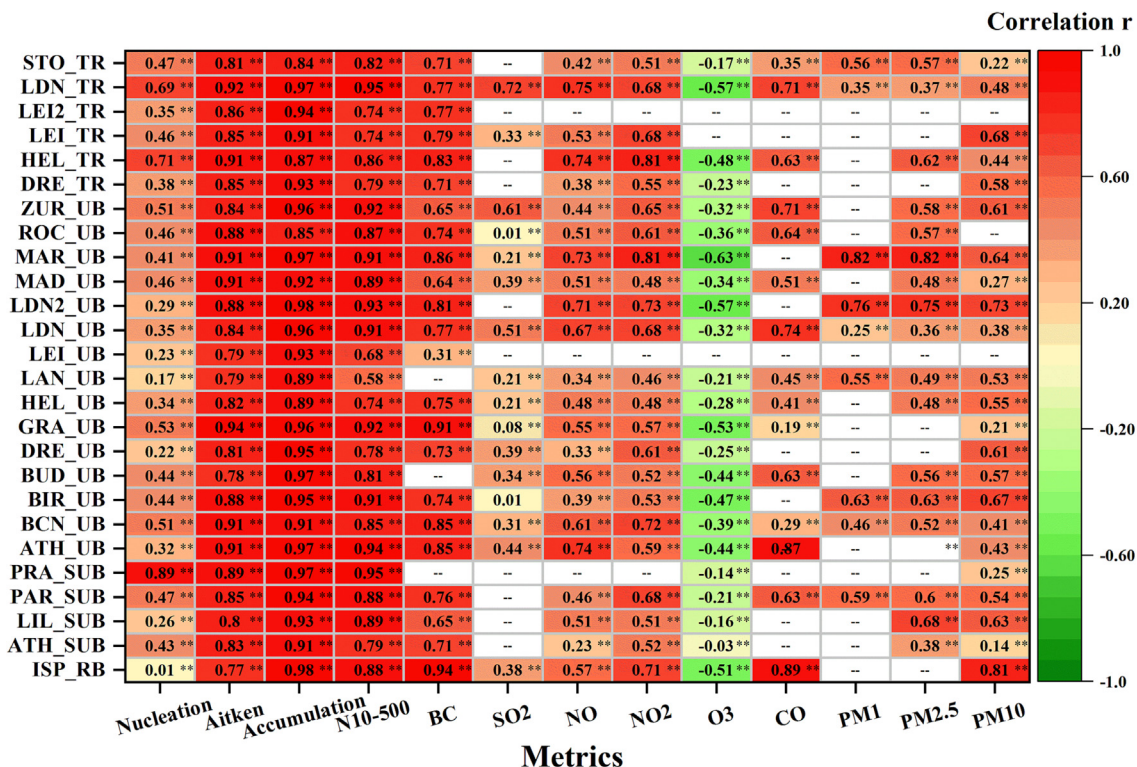
Fig. 5. Pearson's correlation coefficients (r) of total LDSA with fine modes of the nucleation (<25 nm), Aitken (25–100 nm), and smaller size of the accumulation (100–500 nm), PNC_tot (N10–500), BC, gaseous pollutants (SO_2, NO, NO_2, O_3, and CO), and PM_X (PM_1, $PM_{2.5}$, and PM_{10}) individually for the 26 studied sites for the 2017–2019 hourly-averaged concentrations (**$p = 0.01$, and white bands represent missing data).

particles smaller than 400 nm, which is consistent with our findings. Hence, we selected 400 nm as the upper size limit to ensure comparability of datasets. Previous studies have also confirmed that urban vehicle emissions are the main source of fine mode in the urban atmosphere, with particles mainly in the form of soot having prevalent Aitken and accumulation mode sizes (30–500 nm) (Shi et al., 2000; Vu et al., 2015). Meanwhile, Fig. S1 indicates that the contribution of particles smaller than 10 nm to LDSA is relatively low (weight: 0.14 % ± 0.2 %). Our findings show that there is a stronger correlation between LDSA and PNC in the nucleation and Aitken mode at TR sites compared to what is observed at UB and SUB stations. This correlation suggests that there is a stronger association between LDSA and traffic-related particle sources at urban traffic stations. Conversely, in the accumulation mode, there is a higher correlation between LDSA and PNC at SUB sites compared to what is observed at UB and TR sites. This implies that there is a stronger correlation between LDSA and particle sources associated with industrial and other human activities at SUB stations.

3.3.2. Total LDSA vs BC

In 2012, the International Agency for Research on Cancer (IARC) classified BC-containing diesel soot as group 1, carcinogenic to humans (IARC, 2012). Although previous studies have analyzed the correlation between BC and ALV-LDSA (Liu et al., 2022; Reche et al., 2015), the correlation between the two indicators at different monitoring sites has not been investigated in detail. However, it has also been reported that the relationship between BC and LDSA is important for understanding particle health impacts and for source apportionment (Lepistö et al., 2022). In this study, the concentrations of total LDSA and BC are correlated ($p = 0.01$) at all 26 monitoring stations (Fig. 5), and particularly at the sites ISP_RB, PRA_SUB, ATH_UB, BUD_UB, GRA_UB, LAN_UB, LDN_UB, and ROC_UB, where the correlation coefficients are >0.8. This result suggests that a significant fraction of BC is located in the UFPs, and they may have similar prevailing sources and the same particle size range (Chang et al., 2022; Kumar et al., 2010; Lepistö et al., 2022). While at site LEI_UB, the correlation

between LDSA and BC was relatively low, with an r^2 of 0.096. This was primarily due to the fact that the highest PNC was recorded during non-peak traffic hours, around 11–12 h, and anti-correlated with BC. Specifically, PNC reached its maximum at midday, whereas BC was at its lowest point during midday and peaked during traffic rush hours. The observed pattern could be attributed to regional or urban photo-nucleation and fumigation from higher atmospheric layers, which are enriched in nucleation mode and O_3 and depleted in BC as the planetary boundary layer grows through convective dynamics (Trechera et al., 2023).

In urban areas of Europe, aerosols containing BC mostly arise from both aged and fresh road traffic particles and include long-range transported as well as locally generated traffic particles (Saarikoski et al., 2021; Zeka et al., 2006). Therefore, the high correlation of between total LDSA and BC implies that the traffic emission made a high contribution to total LDSA.

3.3.3. Total LDSA vs gaseous pollutants

A correlation analysis between total LDSA concentrations at each site and the concentrations of gaseous pollutants (SO_2, CO, NO, NO_2, and O_3) has been carried out. The results show a moderate and positive correlation between total LDSA and SO_2 ($0.00 \leq r^2 \leq 0.52$), NO ($0.05 \leq r^2 \leq 0.56$), NO_2 ($0.21 \leq r^2 \leq 0.64$), and CO ($0.02 \leq r^2 \leq 0.79$) (Fig. 5). Since CO, NO, and NO_2 mostly arise from the combustion of fossil fuels (all four pollutants), including that from motor vehicle emissions (mainly NO, NO_2 and CO) (Liu et al., 2021a, Liu et al., 2021b), which points to total LDSA as a tracer of road traffic emissions. To confirm this phenomenon, the correlation between LDSA and gaseous pollutants were compared in different type area. We found the higher correlation at traffic sites, supporting with our finding. In particular, at sites ISP_RB and LIL_SUB, LDSA vs CO, the r^2 values were 0.79 and 0.76, respectively, implying that the main source of LDSA at these two sites is from vehicle emissions. Total LDSA concentrations are negatively correlated with O_3 concentrations at all sites ($-0.63 \leq r \leq -0.03$). These negative values are likely the result of the inverse relationship between O_3 and NO_X due to the titration of O_3 by NO (Cao et al., 2022).

3.3.4. Total LDSA vs PM_X

The correlations between total LDSA and ambient PM_X (PM_1, $PM_{2.5}$, and PM_{10}) are highly variable among the sites (Fig. 5). For example, in DRE_UB, ISP_RB, LIL_UB, LDN2_UB, and MAR_UB, r is >0.60, and reaches 0.88 in one case, while in MAD_UB, DRE_UB and GRA_UB, r is <0.20. The results show clearly that levels of PM_X do not necessarily co-vary with those of LDSA and hence it is possible that the measurements of the latter can significantly improve the ability of air quality monitoring to evaluate the harmful effects of particulate pollution (Salo et al., 2021a, Salo et al., 2021b).

4. Conclusions and limitations

This study analyzes the long-term (2017–2019) spatial-temporal characteristics of total LDSA at 25 European and one USA monitoring sites, including 15 urban backgrounds, UB; four suburban backgrounds, SUB; one regional background, RB; and six traffic, TR, sites. The concentration of total LDSA varies across urban Europe. The annual range of concentration for all sites is between 20 and 85 $\mu m^2/cm^3$. There are lower UB concentrations in Northern Europe and higher concentrations in Southern Europe, with a trend of TR > UB > SUB. The diel, weekly, and seasonal variability in total LDSA shows significant differences ($p = 0.01$) at different types of sites, which may be caused by the changes in the sources of UFP and larger particles, emission rates, traffic volume, and meteorological factors, including those favoring new particle formation, stagnation, long-range transport, vertical transport of aerosols, and influence from plumes from pollution hotspots. Based on the correlations of total LDSA with other pollutant metrics, it is suggested that the PNC in the Aitken and accumulation modes are mainly associated with the total LDSA concentration. The results also indicated that the main proportion of LDSA is attributed to the ALV (50 % on average at all sites), followed by the TB (34 %) and HA (16 %) fractions. Overall, the results of this study provide valuable information on the total LDSA concentrations in different types of locations and highlights the importance of considering LDSA as an additional air quality indicator due to its possible relationship with health risks. The evaluation of total LDSA as an exposure metric in time series of epidemiological studies should be further investigated.

The direct comparison of the datasets was a major limitation due to different protocols used for PNSD measurements and quality assurance. Some datasets (DRE_UB, LAN_UB, LEI_UB, DRE_TR, LEI and LEI2_TR) were obtained following the ACTRIS protocols for measurements of PNSD and the instruments are frequently passing quality assurance exercises by the World Calibration Center for Aerosol Physics (WCCAP, https://www.eurochamp.org/calibration-centres/wccap), while others (ATH_UB, BCN_UB, GRA_UB, HEL_UB, MAD_UB, HEL_TR, ATH_SUB, LIL_SUB, PRA_SUB, ISP_RB) are produced by ACTRIS collaborators or partners and are obtained with protocols tending to follow the ones from ACTRIS, but not recently or never passed the quality checks by WCCAP. Finally, datasets of BIR_UB, BUD_UB, LND and LND2_UB, MAR_UB, ROC_UB, ZUR_UB, PAR_SUB, LND_TR and STO_TR are obtained by highly specialized research teams, but data uncertainty remains unknown. The lack of harmonization has caused a high variability of the lower size detection limit, with some PNSD measurements starting from 3 nm, while others start at 20 nm. Accordingly, caution is required when comparing LDSA values from these end member sites. However, one should take into account that LDSA contributions below 10 nm are relatively small.

CRediT authorship contribution statement

Data availability

Data will be made available on request.

Declaration of competing interest

The authors declare that they have no known competing financial interests or personal relationships that could have appeared to influence the work reported in this paper.

Acknowledgements

Appendix A. Supplementary data

Supplementary data to this article can be found online at https://doi.org/10.1016/j.scitotenv.2023.165466.

References

Abdillah, S.F., Wang, Y., 2022. Ambient ultrafine particle (pm0. 1): sources, characteristics, measurements and exposure implications on human health. Environ. Res. 115061.

Allan, J.D., Williams, P.I., Morgan, W.T., Martin, C.L., Flynn, M.J., Lee, J., Nemitz, E., Phillips, G.J., Gallagher, M.W., Coe, H., 2010. Contributions from transport, solid fuel burning and cooking to primary organic aerosols in two Uk cities. Atmos. Chem. Phys. 10 (2), 647–668.

Asbach, C., Kaminski, H., Fissan, H., Monz, C., Dahmann, D., Mülhopt, S., Paur, H.R., Kiesling, H.J., Herrmann, F., Voetz, M., 2009. Comparison of four mobility particle sizers with different time resolution for stationary exposure measurements. J. Nanopart. Res. 11 (7), 1593–1609.

Asgharian, B., 2022. Multiple Path Particle Dosimetry (Mppd) Model and its Applications.

Baldauf, R.W., Devlin, R.B., Gehr, P., Giannelli, R., Hassett-Sipple, B., Jung, H., Martini, G., Mcdonald, J., Sacks, J.D., Walker, K., 2016. Ultrafine particle metrics and research considerations: review of the 2015 ufp workshop. Int. J. Environ. Res. Public Health 13 (11), 1054.

Bari, M., Baumbach, G., Kuch, B., Scheffknecht, G., 2010. Particle-phase concentrations of polycyclic aromatic hydrocarbons in ambient air of rural residential areas in southern Germany. Air Quality, Atmosphere & Health 3 (2), 103–116.

Cao, X., Liu, X., Hadiatullah, H., Xu, Y., Zhang, X., Bendl, J., Cyrys, J., Zimmermann, R., Adam, T., 2022. Investigation of covid-19-related lockdowns on the air pollution changes in Augsburg in 2020, Germany. Atmos Pollut Res 13 (9), 101536. https://doi.org/10.1016/j.apr.2022.101536.

Cassee, F., Morawska, L., Peters, A., Wierzbicka, A., Buonanno, G., Cyrys, J., SchnelleKreis, J., Kowalski, M., Riediker, M., Birmili, W., Querol, X., 2019. Ambient ultrafine particles: evidence for policy makers. Thinking Outside the Box. Report. 1, pp. 1–19.

Chang, P., Griffith, S.M., Chuang, H., Chuang, K., Wang, Y., Chang, K., Hsiao, T., 2022. Particulate matter in a motorcycle-dominated urban area: source apportionment and cancer risk of lung deposited surface area (ldsa) concentrations. J. Hazard. Mater. 427, 128188. https://doi.org/10.1016/j.jhazmat.2021.128188.

Chen, R., Hu, B., Liu, Y., Xu, J., Yang, G., Xu, D., Chen, C., 2016. Beyond pm2. 5: the role of ultrafine particles on adverse health effects of air pollution. Biochimica et Biophysica Acta (BBA)-General Subjects 1860 (12), 2844–2855.

Cheristanidis, S., Grivas, G., Chaloulakou, A., 2020. Determination of total and lung-deposited particle surface area concentrations, in Central Athens, Greece. Environ. Monit. Assess. 192 (10), 627. https://doi.org/10.1007/s10661-020-08569-8.

Duncan, D.B., 1955. Multiple range and multiple f tests. Biometrics 11 (1), 1–42.

Faridi, S., Niazi, S., Yousefian, F., Azimi, F., Pasalari, H., Momeniha, F., Mokammel, A., Gholampour, A., Hassanvand, M.S., Naddafi, K., 2019. Spatial homogeneity and heterogeneity of ambient air pollutants in Tehran. Sci. Total Environ. 697, 134123.

Fierz, M., Houle, C., Steigmeier, P., Burtscher, H., 2011. Design, calibration, and field performance of a miniature diffusion size classifier. Aerosol Sci. Technol. 45 (1), 1–10.

Fung, P.L., Zaidan, M.A., Niemi, J.V., Saukko, E., Timonen, H., Kousa, A., Kuula, J., Rönnkö, T., Karppinen, A., Tarkoma, S., 2022. Input-adaptive linear mixed-effects model for estimating alveolar lung-deposited surface area (ldsa) using multipollutant datasets. Atmos. Chem. Phys. 22 (3), 1861–1882.

Gonzalez, A., Boies, A., Swanson, J., Kittelson, D., 2022. Measuring the air quality using low-cost air sensors in a parking garage at university of Minnesota, Usa. Int. J. Environ. Res. Public Health 19 (22), 15223.

Hama, S.M.L., Ma, N., Cordell, R.L., Kos, G.P.A., Wiedensohler, A., Monks, P.S., 2017. Lung deposited surface area in Leicester urban background site/Uk: sources and contribution of new particle formation. Atmos. Environ. 1994 (151), 94–107. https://doi.org/10.1016/j.atmosenv.2016.12.002.

Hammer, T., Fissan, H., Wang, J., 2019. Determination of the delivered dose of nanoparticles in the tracheabronchial and alveolar regions of the lung. Nanoimpact. 14, 100162.

Harrison, R.M., Shi, J.P., Xi, S., Khan, A., Mark, D., Kinnersley, R., Yin, J., 2000. Measurement of number, mass and size distribution of particles in the atmosphere. Philosophical transactions of the Royal Society of London. Series A: Mathematical, Physical and Engineering Sciences 358 (1775), 2567–2580.

Helin, A., Niemi, J.V., Virkkula, A., Pirjola, L., Teinilä, K., Backman, J., Aurela, M., Saarikoski, S., Rönnkö, T., Asmi, E., 2018. Characteristics and source apportionment of black carbon in the Helsinki metropolitan area, Finland. Atmos. Environ. 1994 (190), 87–98.

Hietikko, R., Kuuluvainen, H., Harrison, R.M., Portin, H., Timonen, H., Niemi, J.V., Rönnkö, T., 2018. Diurnal variation of nanocluster aerosol concentrations and emission factors in a street canyon. Atmos. Environ. 1994 (189), 98–106.

Hussein, T., Löndahl, J., Paasonen, P., Koivisto, A.J., Petäjä, T., Hämeri, K., Kulmala, M., 2013. Modeling regional deposited dose of submicron aerosol particles. Sci. Total Environ. 458-460, 140–149. https://doi.org/10.1016/j.scitotenv.2013.04.022.

Hussein, T., Wierzbicka, A., Löndahl, J., Lazaridis, M., Hänninen, O., 2015. Indoor aerosol modeling for assessment of exposure and respiratory tract deposited dose. Atmos. Environ. 1994 (106), 402–411. https://doi.org/10.1016/j.atmosenv.2014.07.034.

Hussein, T., Al-Abdallat, A., Saleh, S.S.A., Al-Kloub, M., 2022. Estimation of the seasonal inhaled deposited dose of particulate matter in the respiratory system of urban individuals living in an eastern mediterranean city. Int. J. Environ. Res. Public Health 19 (7), 4303.

Junkermann, W., Vogel, B., Bangert, M., 2016. Ultrafine particles over Germany–an aerial survey. Tellus B: Chemical and Physical Meteorology 68 (1), 29250.

Katsanos, D., Bougiatioti, A., Liakakou, E., Kaskaoutis, D., Stavroulas, I., Paraskevopoulou, D., Lianou, M., Psiloglou, B.E., Gerasopoulos, E., Pilinis, C., 2019. Optical properties of near-surface urban aerosols and their chemical tracing in a mediterranean city (Athens). Aerosol Air Qual. Res. 19 (1), 49–70.

Khan, I., Zakari, A., Ahmad, M., Irfan, M., Hou, F., 2022. Linking energy transitions, energy consumption, and environmental sustainability in oecd countries. Gondwana Res. 103, 445–457.

Kruskal, W.H., Wallis, W.A., 1952. Use of ranks in one-criterion variance analysis. J. Am. Stat. Assoc. 47 (260), 583–621.

Kumar, P., Robins, A., Vardoulakis, S., Britter, R., 2010. A review of the characteristics of nanoparticles in the urban atmosphere and the prospects for developing regulatory controls. Atmos Environ (1994) 44 (39), 5035–5052.

Kumar, P., Morawska, L., Birmili, W., Paasonen, P., Hu, M., Kulmala, M., Harrison, R.M., Norford, L., Britter, R., 2014. Ultrafine particles in cities. Environ. Int. 66, 1–10.

Kuula, J., Kuuluvainen, H., Niemi, J.V., Saukko, E., Portin, H., Kousa, A., Aurela, M., Rönnkö, T., Timonen, H., 2020. Long-term sensor measurements of lung deposited surface area of particulate matter emitted from local vehicular and residential wood combustion sources. Aerosol Sci. Technol. 54 (2), 190–202. https://doi.org/10.1080/02786826.2019.1668909.

Kuuluvainen, H., Rönnkö, T., Järvinen, A., Saari, S., Karjalainen, P., Lähde, T., Pirjola, L., Niemi, J.V., Hillamo, R., Keskinen, J., 2016. Lung deposited surface area size distributions of particulate matter in different urban areas. Atmos. Environ. 1994 (136), 105–113. https://doi.org/10.1016/j.atmosenv.2016.04.019.

Kwon, H., Ryu, M.H., Carlsten, C., 2020. Ultrafine particles: unique physicochemical properties relevant to health and disease. Exp. Mol. Med. 52 (3), 318–328.

Lampilahti, J., Leino, K., Manninen, A., Poutanen, P., Franck, A., Peltola, M., Hietala, P., Beck, L., Dada, L., Quéléver, L., 2021. Aerosol particle formation in the upper residual layer. Atmos. Chem. Phys. 21 (10), 7901–7915.

Lepistö, T., Kuuluvainen, H., Lintusaari, H., Kuittinen, N., Salo, L., Helin, A., Niemi, J.V., Manninen, H.E., Timonen, H., Jalava, P., 2022. Connection between lung deposited surface area (ldsa) and black carbon (bc) concentrations in road traffic and harbour environments. Atmos. Environ. 1994, 118931.

Li, J., Xu, W., Li, Z., Duan, M., Ouyang, B., Zhou, S., Lei, L., He, Y., Sun, J., Wang, Z., 2021. Real-time characterization of aerosol particle composition, sources and influences of increased ventilation and humidity in an office. Indoor Air 31 (5), 1364–1376.

Liu, X., Hadiatullah, H., Tai, P., Xu, Y., Zhang, X., Schnelle-Kreis, J., Schloter-Hai, B., Zimmermann, R., 2021a. Air pollution in Germany: spatio-temporal variations and their driving factors based on continuous data from 2008 to 2018. Environ. Pollut. 276, 116732. https://doi.org/10.1016/j.envpol.2021.116732.

Liu, X., Zhang, X., Schnelle-Kreis, J., Jakobi, G., Cao, X., Cyrys, J., Yang, L., Schloter-Hai, B., Abbaszade, G., Orasche, J., Khedr, M., Kowalski, M., Hank, M., Zimmermann, R., 2021b. Spatiotemporal characteristics and driving factors of black carbon in Augsburg, Germany: combination of mobile monitoring and street view images. Environ. Sci. Technol. 55 (1), 160–168. https://doi.org/10.1021/acs.est.0c04776.

Liu, X., Hadiatullah, H., Khedr, M., Zhang, X., Schnelle-Kreis, J., Zimmermann, R., Adam, T., 2022. Personal exposure to various size fractions of ambient particulate matter during the heating and non-heating periods using mobile monitoring approach: a case study in Augsburg, Germany. Atmos Pollut Res 101483.

Liu, Y., Wu, L., Huang, S., Song, Q., Hu, W., Chen, W., Wu, Z., Man, R., He, Y., Li, W., Peng, Y., Liu, J., Song, W., Ma, N., Yuan, B., Wang, X., Shao, M., 2023. Sources, size-resolved deposition in the human respiratory tract and health risks of submicron black carbon in urban atmosphere in pearl river delta, China. Sci. Total Environ. 891, 164391. https://doi.org/10.1016/j.scitotenv.2023.164391.

Mahowald, N., Albani, S., Kok, J.F., Engelstaeder, S., Scanza, R., Ward, D.S., Flanner, M.G., 2014. The size distribution of desert dust aerosols and its impact on the earth system. Aeolian Res. 15, 53–71.

Masiol, M., Squizzato, S., Chalupa, D.C., Utell, M.J., Rich, D.Q., Hopke, P.K., 2018. Long-term trends in submicron particle concentrations in a metropolitan area of the northeastern United States. Sci. Total Environ. 633, 59–70.

Mcdonald, R., Biswas, P., 2004. A methodology to establish the morphology of ambient aerosols. J Air Waste Manag Assoc 54 (9), 1069–1078.

Mcmurry, P.H., 2000. A review of atmospheric aerosol measurements. Atmos Environ (1994) 34 (12–14), 1959–1999.

Niemi, J.V., Saarikoski, S., Aurela, M., Tervahattu, H., Hillamo, R., Westphal, D.L., Aarnio, P., Koskentalo, T., Makkonen, U., Vehkamäki, H., 2009. Long-range transport episodes of fine particles in southern Finland during 1999–2007. Atmos Environ (1994) 43 (6), 1255–1264.

Petzold, A., Hasselbach, J., Lauer, P., Baumann, R., Franke, K., Gurk, C., Schlager, H., Weingartner, E., 2008. Experimental studies on particle emissions from cruising ship, their characteristic properties, transformation and atmospheric lifetime in the marine boundary layer. Atmos. Chem. Phys. 8 (9), 2387–2403.

Rao, X., Zhong, J., Brook, R.D., Rajagopalan, S., 2018. Effect of particulate matter air pollution on cardiovascular oxidative stress pathways. Antioxid. Redox Signal. 28 (9), 797–818.

Reche, C., Viana, M., Brines, M., Pérez, N., Beddows, D., Alastuey, A., Querol, X., 2015. Determinants of aerosol lung-deposited surface area variation in an urban environment. Sci. Total Environ. 517, 38–47. https://doi.org/10.1016/j.scitotenv.2015.02.049.

Reddy, B.S.K., Kumar, K.R., Balakrishnaiah, G., Gopal, K.R., Reddy, R.R., Reddy, L., Ahammed, Y.N., Narasimhulu, K., Moorthy, K.K., Babu, S.S., 2012. Potential source regions contributing to seasonal variations of black carbon aerosols over Anantapur in Southeast India. Aerosol Air Qual. Res. 12 (3), 344–358.

Rivas, I., Beddows, D.C., Amato, F., Green, D.C., Järvi, L., Hueglin, C., Reche, C., Timonen, H., Fuller, G.W., Niemi, J.V., 2020. Source apportionment of particle number size distribution in urban background and traffic stations in four european cities. Environ. Int. 135, 105345.

Saarikoski, S., Niemi, J.V., Aurela, M., Pirjola, L., Kousa, A., Rönnkö, T., Timonen, H., 2021. Sources of black carbon at residential and traffic environments obtained by two source apportionment methods. Atmos. Chem. Phys. 21 (19), 14851–14869.

Salma, I., Füri, P., Németh, Z., Balásházy, I., Hofmann, W., Farkas, Á., 2015. Lung burden and deposition distribution of inhaled atmospheric urban ultrafine particles as the first step in their health risk assessment. Atmos. Environ. 1994 (104), 39–49.

Salma, I., Németh, Z., Weidinger, T., Kovács, B., Kristóf, G., 2016. Measurement, growth types and shrinkage of newly formed aerosol particles at an urban research platform. Atmos. Chem. Phys. 16 (12), 7837–7851.

Salma, I., Varga, V., Németh, Z., 2017. Quantification of an atmospheric nucleation and growth process as a single source of aerosol particles in a city. Atmos. Chem. Phys. 17 (24), 15007–15017.

Salma, I., Vasanits-Zsigrai, A., Machon, A., Varga, T., Major, I., Gergely, V., Molnár, M., 2020. Fossil fuel combustion, biomass burning and biogenic sources of fine carbonaceous aerosol in the carpathian basin. Atmos. Chem. Phys. 20 (7), 4295–4312.

Salo, L., Hyvärinen, A., Jalava, P., Teinilä, K., Hooda, R.K., Datta, A., Saarikoski, S., Lintusaari, H., Lepistö, T., Martikainen, S., 2021a. The characteristics and size of lung-depositing particles vary significantly between high and low pollution traffic environments. Atmos environ (1994) 255, 118421.

Salo, L., Rönkkö, T., Saarikoski, S., Teinilä, K., Kuula, J., Alanen, J., Arffman, A., Timonen, H., Keskinen, J., 2021b. Concentrations and size distributions of particle lung-deposited surface area (ldsa) in an underground mine. Aerosol Air Qual. Res. 21 (8), 200660.

Schmid, O., Stoeger, T., 2016. Surface area is the biologically most effective dose metric for acute nanoparticle toxicity in the lung. J. Aerosol Sci. 99, 133–143.

Seinfeld, J., Pandis, S., 2008. Atmospheric chemistry and physics. 1997. New York.

Shi, J.P., Mark, D., Harrison, R.M., 2000. Characterization of particles from a current technology heavy-duty diesel engine. Environ. Sci. Technol. 34 (5), 748–755.

Siegmann, P., Gomez-Moreno, H., 2022. Photoelectric and diffusion charging measurements of fine particulate air pollution along the main roads of the city of Madrid from 1999 to 2021. Atmos environ (1994) 282, 119160.

Sioutas, C., Delfino, R.J., Singh, M., 2005. Exposure assessment for atmospheric ultrafine particles (ufps) and implications in epidemiologic research. Environ. Health Perspect. 113 (8), 947–955.

Sun, J., Birmili, W., Hermann, M., Tuch, T., Weinhold, K., Spindler, G., Schladitz, A., Bastian, S., Löschau, G., Cyrys, J., Gu, J., Flentje, H., Briel, B., Asbach, C., Kaminski, H., Ries, L., Sohmer, R., Gerwig, H., Wirtz, K., Meinhardt, F., Schwerin, A., Bath, O., Ma, N., Wiedensohler, A., 2019. Variability of black carbon mass concentrations, submicrometer particle number concentrations and size distributions: results of the german ultrafine aerosol network ranging from city street to high alpine locations. Atmos. Environ. 1994 (202), 256–268. https://doi.org/10.1016/j.atmosenv.2018.12.029.

Teinilä, K., Aurela, M., Niemi, J.V., Kousa, A., Petäjä, T., Järvi, L., Hillamo, R., Kangas, L., Saarikoski, S., Timonen, H., 2019. Concentration Variation of Gaseous and Particulate Pollutants in the Helsinki City Centre—Observations from a Two-Year Campaign from 2013–2015. Boreal Environ Res.

Thén, W., Salma, I., 2022. Particle number concentration: a case study for air quality monitoring. Atmosphere (Basel) 13 (4), 570.

Todea, A.M., Beckmann, S., Kaminski, H., Asbach, C., 2015. Accuracy of electrical aerosol sensors measuring lung deposited surface area concentrations. J. Aerosol Sci. 89, 96–109. https://doi.org/10.1016/j.jaerosci.2015.07.003.

Trechera, P., Garcia-Marlès, M., Liu, X., Reche, C., Pérez, N., Savadkoohi, M., Beddows, D., Salma, I., Vörösmarty, M., Casans, A., 2023. Phenomenology of ultrafine particle concentrations and size distribution across urban europe. Environ. Int. 172, 107744.

Vieira, C.L.Z., Koutrakis, P., 2021. The impact of solar activity on ambient ultrafine particle concentrations: an analysis based on 19-year measurements in Boston, Usa. Environ. Res. 201, 111532.

Voliotis, A., Samara, C., 2018. Submicron particle number doses in the human respiratory tract: implications for urban traffic and background environments. Environ. Sci. Pollut. Res. Int. 25 (33), 33724–33735.

Vu, T.V., Delgado-Saborit, J.M., Harrison, R.M., 2015. Particle number size distributions from seven major sources and implications for source apportionment studies. Atmos. Environ. 1994 (122), 114–132.

Wehner, B., Birmili, W., Gnauk, T., Wiedensohler, A., 2002. Particle number size distributions in a street canyon and their transformation into the urban-air background: measurements and a simple model study. Atmos Environ (1994) 36 (13), 2215–2223.

Whitby, K.T., Husar, R.B., Liu, B.Y., 1972. The aerosol size distribution of los angeles smog. J. Colloid Interface Sci. 39 (1), 177–204.

Wiegand, F., Pereira, F.N., Teixeira, E.C., 2011. Study on wet scavenging of atmospheric pollutants in South Brazil. Atmos Environ (1994) 45 (27), 4770–4776.

Wierzbicka, A., Nilsson, P.T., Rissler, J., Sallsten, G., Xu, Y., Pagels, J.H., Albin, M., österberg, K., Strandberg, B., Eriksson, A., 2014. Detailed diesel exhaust characteristics including particle surface area and lung deposited dose for better understanding of health effects in human chamber exposure studies. Atmos. Environ. 1994 (86), 212–219.

Wilson, J.G., Kingham, S., Pearce, J., Sturman, A.P., 2005. A review of intraurban variations in particulate air pollution: implications for epidemiological research. Atmos Environ (1994) 39 (34), 6444–6462. https://doi.org/10.1016/j.atmosenv.2005.07.030.

Xu, J., Yang, W., Bai, Z., Zhang, R., Zheng, J., Wang, M., Zhu, T., 2022. Modeling spatial variation of gaseous air pollutants and particulate matters in a metropolitan area using mobile monitoring data. Environ. Res. 210, 112858.

Yang, W., Deng, M., Xu, F., Wang, H., 2018. Prediction of hourly pm2. 5 using a space-time support vector regression model. Atmos. Environ. (1994) 181, 12–19.

Zeka, A., Sullivan, J.R., Vokonas, P.S., Sparrow, D., Schwartz, J., 2006. Inflammatory markers and particulate air pollution: characterizing the pathway to disease. Int. J. Epidemiol. 35 (5), 1347–1354.

Zhou, B., Wang, Q., Zhou, Q., Zhang, Z., Wang, G., Fang, N., Li, M., Cao, J., 2018. Seasonal characteristics of black carbon aerosol and its potential source regions in Baoji, China. Aerosol Air Qual. Res. 18 (2), 397–406.

Zhu, X., Tang, G., Guo, J., Hu, B., Song, T., Wang, L., Xin, J., Gao, W., Münkel, C., Schäfer, K., 2018. Mixing layer height on the North China plain and meteorological evidence of serious air pollution in southern Hebei. Atmos. Chem. Phys. 18 (7), 4897–4910.